Supporting Information

Single-Crystal-to-Single-Crystal MOF Encapsulation of Copper Azide to Prepare Laser-sensitive Primary Explosive

Ruibing Lv,[a] Pengyang Pan,[a] Zhenghang Luo,[a] Ying Wang,[a] Quancheng Liu,[b] Hu Deng,*[b] and Qi Zhang,*[a]

[a] Institute of Chemical Materials (ICM), China Academy of Engineering Physics (CAEP), Mianyang 621900, P. R. China
E-mail: jackzhang531@caep.cn

[b] School of Information Engineering, Southwest University of Science and Technology, Mianyang 621010, P. R. China

Table of Contents

1. Experimental Section

Caution! Although there was no accidental explosion during the synthesis and treatment process, $[Cu(ATRZ)_3(NO_3)_2]_n$, ATRZ, sodium azide, and $[Cu(ATRZ)(N_3)_2]_n$ are energetic materials. Appropriate safety precautions should be taken in every research process of energetic materials. Leather coats, latex gloves, eye-protecting glasses, earplugs, and face shields are recommended for the whole experimental process. The impacts, friction and electrostatic of energetic materials must be avoided.

Reagents and General Methods: Acetic acid (99.5%, AR), 4-amino-1,2,4-triazole (98.0%, AR), sodium dichloroisocyanurate (96.0%), Copper nitrate trihydrate (99%, AR), and sodium azide (99%) were purchased from Shanghai Aladdin Biochemical Technology Co., Ltd. Infrared (IR) spectra were performed on the Perkin-Elmer Spectrum II IR Spectrometers using KBr pellets. The powder X-ray diffraction patterns were collected on a Bruker D8 Advance, and the 2θ range measured was 5-50° with steps of 0.02°/0.1s. The single crystal data were collected using an Oxford Diffraction Xcalibur, the structures were solved and refined with the SHELXS program in the Olex2/1.2 software suite. Thermogravimetric and differential scanning calorimetry analysis (TG-DSC) curves were recorded on a Mettler Toledo calorimeter equipped with an auto-cooling accessory at a scan rate of 10 K min^{-1}. Impact and friction sensitivity data were measured using a standard BAM Fall hammer and a BAM friction tester.

Synthesis of 4,4'-azo-1,2,4-triazole (ATRZ): Sodium dichloroisocyanurate (20.12 g, 96 mmol) was dissolved in 200 mL of deionized water at room temperature with stirring until complete dissolution. Subsequently, 10 mL of acetic acid was added, and the mixture was vigorously stirred at room temperature for 4 hours, maintaining the reaction temperature below 10 °C using an ice bath. Separately, 4-amino-1,2,4-triazole (10.1 g, 120 mmol) was dissolved in 10 mL of water and added to the reaction mixture. Stirring was continued for an additional 5 hours to ensure completion of the reaction. The reaction mixture was then filtered, and the solid obtained was dissolved in 300 mL of deionized water by boiling. After cooling for 3 hours, the solution was filtered again to isolate needle-shaped crystals of ATRZ. Yield: 5.12 g, 52%.

Synthesis of $[Cu(ATRZ)_3(NO_3)_2]_n$: ATRZ (15 mmol, 2.5 g) was added to 200 mL of boiling deionized water and added into a 200 mL boiling aqueous solution of $Cu(NO_3)_2·3H_2O$ (4.5 mmol, 1.1 g). The resulting mixture was stirred for 1 hour, followed by filtration. Blue single crystals were obtained through slow evaporation filtrate over several days. Yield: 2.1 g, 70 %. Synthesis of $[Cu(ATRZ)(N_3)_2]_n$: Add $[Cu(ATRZ)_3(NO_3)_2]_n$ (2 g, 3 mmol) to 120 mL of aqueous sodium azide solution (0.5 mol L^{-1}). After 3 days, brown crystals suitable for X-ray diffraction are obtained, which are then filtered, washed, and dried to obtain final product. Yield: 0.79 g, 85 %. T_d (onset) 209 °C. IR (KBr) v = 3090(w), 2044(s), 1493(m), 1382(w), 1341(w), 1313(w), 1220(w), 1180(m), 1044(m), 880(m), 700(m), 616(s), 555(m) cm^{-1}. Anal. calcd for $C_4H_4CuN_{14}$ (311.72 g mol^{-1}): C 15.41, H 1.29, N 62.91; found: C 15.38, H 1.30, N 62.93.
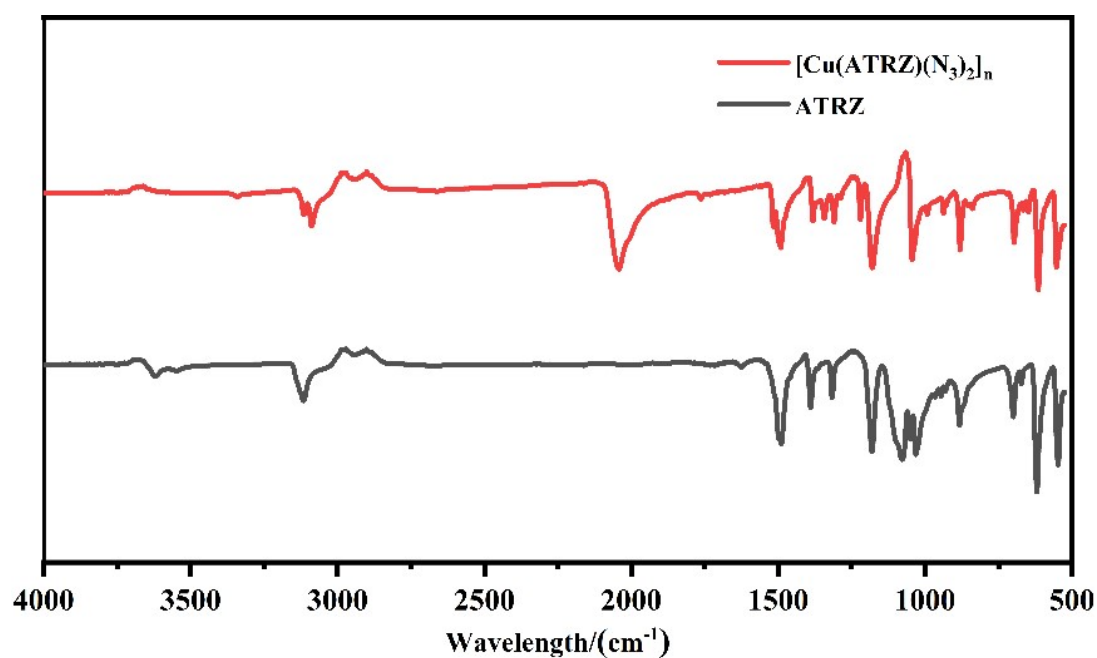
2. FTIR spectroscopy

Fig. S1 IR Curves of ATRZ and $[Cu(ATRZ)(N_3)_2]_n$ (CA-ATRZ).
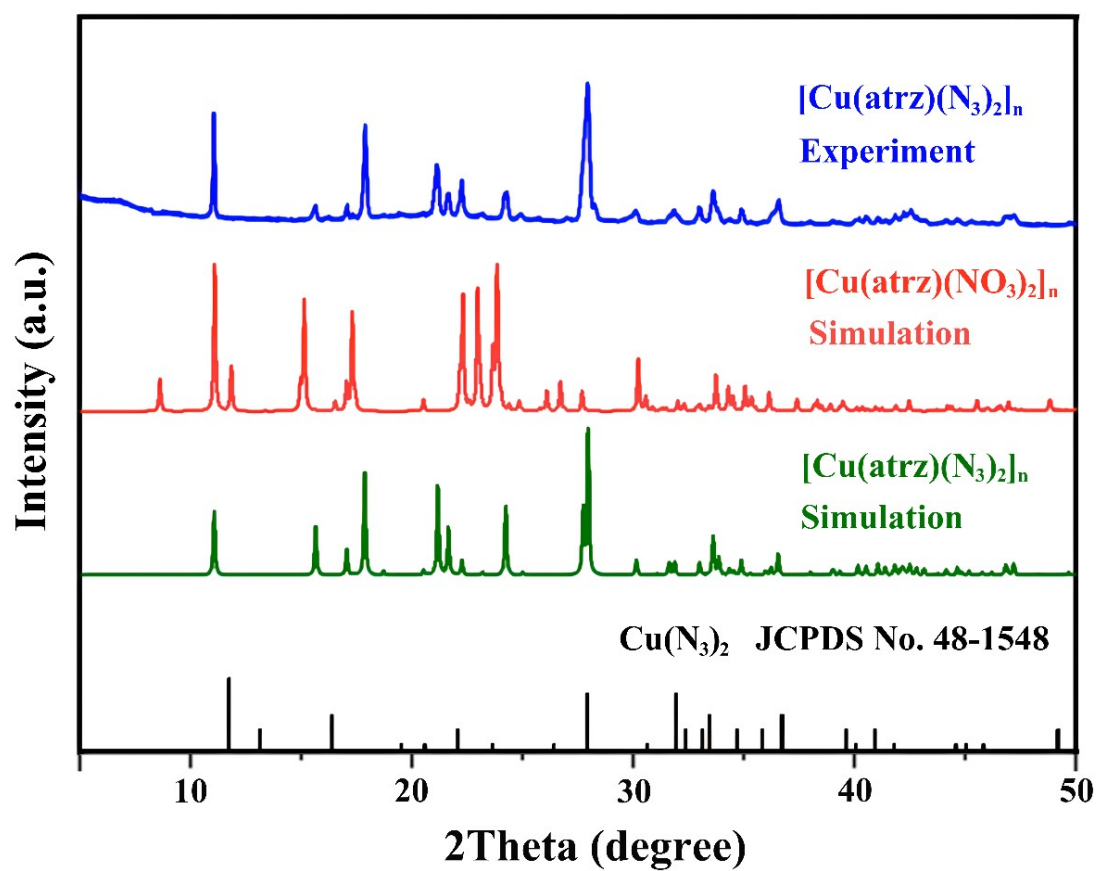

3. Powder X-ray diffraction (PXRD) spectra

Fig. S2 PXRD spectra of CA-ATRZ, $[Cu(ATRZ)_3(NO_3)_2]_n$, and $Cu(N_3)_2$ (CA).

4. X-ray Crystallography

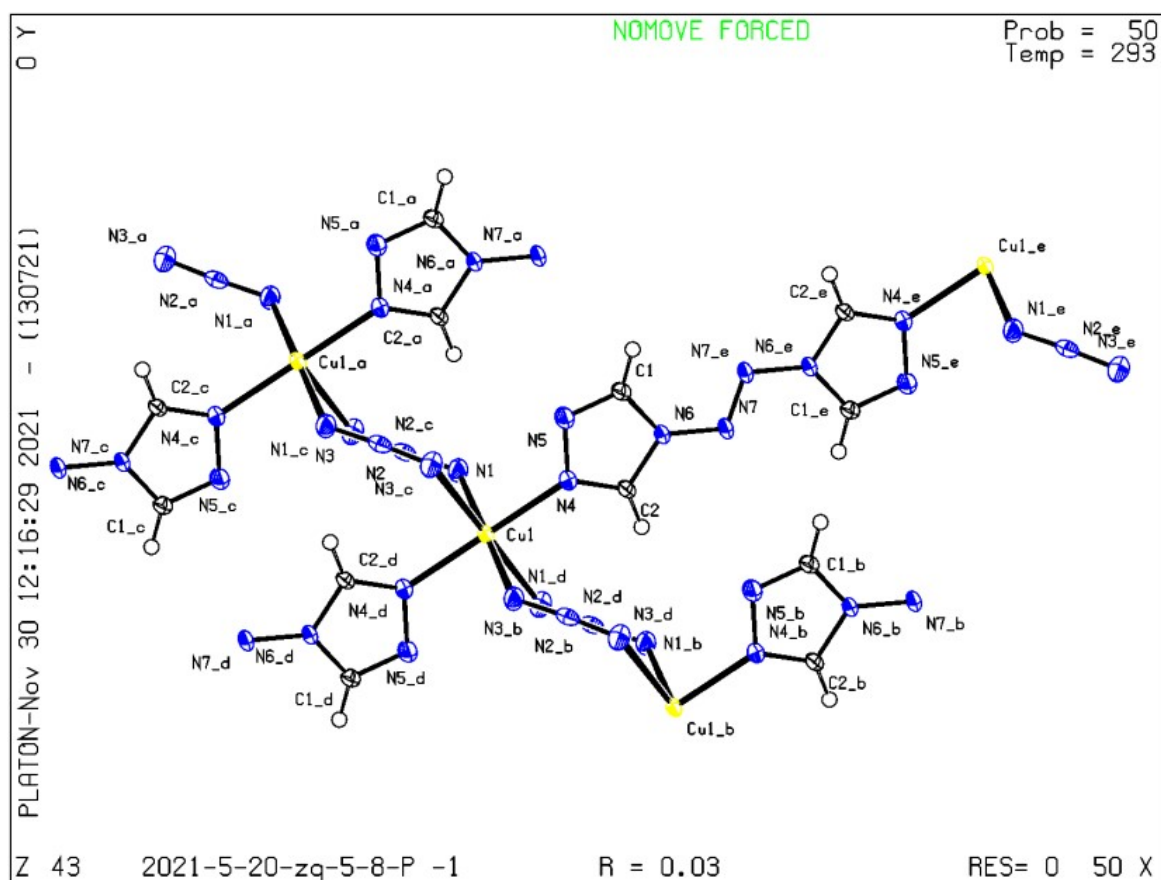**Fig. S3** The crystal structure of $[Cu(ATRZ)(N_3)_2]_n$ (CA-ATRZ).

Table S1. Crystal data and structure refinement for [Cu(ATRZ)(N$_3$)$_2$]$_n$ (CA-ATRZ).

Compounds	[Cu(ATRZ)(N$_3$)$_2$]$_n$ (CA-ATRZ)
CCDC number	2341002
Empirical formula	C$_4$H$_4$CuN$_{14}$
Formula weight	311.75
Temperature/K	293(2)
Crystal system	triclinic
Space group	*P*-1
a/Å	5.2475(6)
b/Å	5.9713(7)
c/Å	8.5316(11)
α/°	73.990(11)
β/°	73.570(11)
γ/°	76.141(10)
Volume/Å^3	242.66(5)
Z	1
ρ$_{calc}$g/cm^3	2.133
μ/mm^{-1}	2.268
F(000)	155.0
Crystal size/mm^3	0.1 × 0.1 × 0.05
Radiation	Mo Kα (λ = 0.71073)
2Θ range for data collection/°	7.21 to 57.466
Index ranges	-6 ≤ h ≤ 6, -7 ≤ k ≤ 7, -11 ≤ l ≤ 11
Reflections collected	3401
Independent reflections	1127 [R$_{int}$ = 0.0422, R$_{sigma}$ = 0.0532]
Data/restraints/parameters	1127/0/88
Goodness-of-fit on F^2	1.036
Final R indexes [I>=2σ (I)]	R$_1$ = 0.0331, wR$_2$ = 0.0699
Final R indexes [all data]	R$_1$ = 0.0400, wR$_2$ = 0.0735
Largest diff. peak/hole / e Å^{-3}	0.44/-0.35

Table S2. Selected bond lengths [Å] for [Cu(ATRZ)(N$_3$)$_2$]$_n$ (CA-ATRZ).

Atom	Atom	Length/Å	Atom	Atom	Length/Å
Cu1	N4	2.036(2)	C2	H2	0.93
Cu1	N1	1.979(2)	N3	Cu1	2.609
Cu1	N3	2.609	C1	H1	0.93
Cu1	N4	2.036(2)	N4	N5	1.397(3)
Cu1	N1	1.979(2)	N4	C2	1.302(5)
Cu1	N3	2.609	N4	Cu1	2.036
N4	N5	1.397(3)	N6	N7	1.392(4)
N4	C2	1.302(5)	N6	C2	1.360(4)
N6	N7	1.392(4)	N6	C1	1.369(4)

N6	C2	1.360(4)	N5	C1	1.301(4)
N6	C1	1.369(4)	C2	H2	0.93
N2	N1	1.189(4)	C1	H1	0.93
N2	N3	1.166(4)	N2	N1	1.189(4)
N7	N7	1.233(3)	N2	N3	1.166(4)
N5	C1	1.301(4)	N1	Cu1	1.979(2)

Table S3. Selected bond Angles [°] for [Cu(ATRZ)(N$_3$)$_2$]$_n$ (CA-ATRZ).

Atom	Atom	Atom	Angle/°	Atom	Atom	Atom	Angle/°
N4	Cu1	N1	86.9	N4	C2	N6	108.8(2)
N4	Cu1	N3	88.92	N4	C2	H2	125.6
N4	Cu1	N4	180	N6	C2	H2	125.6
N4	Cu1	N1	93.1	N2	N3	Cu1	115.8
N4	Cu1	N3	91.08	N6	C1	N5	109.7(2)
N1	Cu1	N3	89.91	N6	C1	H1	125.1
N1	Cu1	N4	93.1	N5	C1	H1	125.2
N1	Cu1	N1	180	N5	N4	C2	108.5(2)
N1	Cu1	N3	90.09	N5	N4	Cu1	120
N3	Cu1	N4	91.08	C2	N4	Cu1	130.8
N3	Cu1	N1	90.09	N7	N6	C2	121.6(2)
N3	Cu1	N3	180	N7	N6	C1	132.0(2)
N4	Cu1	N1	86.9	C2	N6	C1	106.3(2)
N4	Cu1	N3	88.92	N7	N7	N6	110.2(2)
N1	Cu1	N3	89.91	N4	N5	C1	106.7(2)
Cu1	N4	N5	120	N4	C2	N6	108.8(2)
Cu1	N4	C2	130.8	N4	C2	H2	125.6
N5	N4	C2	108.5(2)	N6	C2	H2	125.6
N7	N6	C2	121.6(2)	N6	C1	N5	109.7(2)
N7	N6	C1	132.0(2)	N6	C1	H1	125.1
C2	N6	C1	106.3(2)	N5	C1	H1	125.2
N1	N2	N3	176.2(3)	N1	N2	N3	176.2(3)
N6	N7	N7	110.2(2)	N2	N1	Cu1	127.1
Cu1	N1	N2	127.1	Cu1	N3	N2	115.8
N4	N5	C1	106.7(2)	N3	Cu1	N1	89.91

5. Heats of formation calculations

The constant pressure reaction heat ($\Delta_c U$) of chelate [Cu(ATRZ)(N$_3$)$_2$]$_n$ (CA-ATRZ) was measured by the oxygen bomb calorimeter, and the value of $\Delta_c U$ is the average of three independent experiment results. Standard molar combustion enthalpy ($\Delta_c H_m^\theta$) can be obtained from the constant pressure reaction heat ($\Delta_c U$) and equation 2. The standard molar combustion enthalpy ($\Delta_f H$) of chelate [Cu(ATRZ)(N$_3$)$_2$]$_n$ (CA-ATRZ) (1752 kJ mol^{-1}) was obtained from $\Delta_c H_m^\theta$ according to equation 3. (CO$_2$(g): -393.51 kJ mol^{-1}; H$_2$O(l): 285.85 kJ mol^{-1}; CuO(s): -155.2 kJ mol^{-1})

$$C_4H_4CuN_{14}\ (s)+5.5O_2(g)=4CO_2(g)+CuO(s)+2H_2O(l)+7N_2(g)\ (1)$$

$$\Delta_c H_m^\theta = \Delta_c U + \Delta n R T \quad (2)$$

$$\Delta_f H_m^\theta = \sum \Delta_f H_m^\theta\ (products) - \Delta_c H_m^\theta \quad (3)$$

$\Delta n = n_g$(products) - n_g(reactants), (n_g is the sum of the total moles of gas in the product or reactant, R= 8.314 J mol^{-1} K^{-1}, T= 298.15 K)

6. Interfragment Charge Transfer (IFCT)

Gaussian16 software was used to perform geometric optimization on CA-ATRZ based on B3LYP density functional and 6-311G* basis set, and the TD-DFT method was used to calculate its excited state and obtain its electronic transition properties. Use the IFCT (interfragment charge transfer) method of the Multiwfn program to quantitatively analyze the amount of electron transfer between each fragment of the molecule in a specific excited state transition, and use the electron density difference (CDD, charge density transfer) diagram between the excited state and the ground state (Fig. 7b), showing the electron density changes of each fragment in a visual form, and finally determining the electronic transition mode. The fragment division is shown in Supplementary Fig. 4, and the calculated electron transfer values of each fragment is shown in Supplementary Table 4. Supplementary Table 5 shows the Intrinsic charge transfer (CT) and local excitation (LE) percentage during the CA-ATRZ excitation process. CT mode is further divided into metal-ligand charge transfer (MLCT, metal-ligand charge transfer), ligand-to-metal charge transfer (LMCT, ligand-metal charge transfer) and charge transfer between ligands (LLCT, ligand-ligand charge transfer), while the LE mode includes metal-centered transitions (MC, metal centered) and intra-ligand or ligand-centered transitions (LC, ligand centered). [1-3]
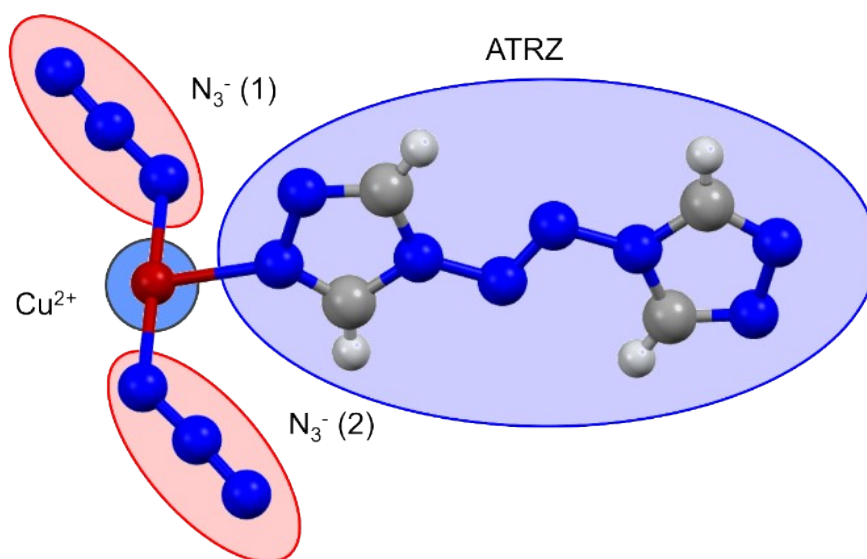
Fig. S4 Fragments division of $[Cu(ATRZ)(N_3)_2]_n$ (CA-ATRZ).

Table S4. Transferred electrons between fragments.

Donors[a]	Receptors[b]			
	Cu^{2+}	N_3 (1)	N_3 (2)	ATRZ (1)
Cu^{2+}	0.10169	0.03276	0.06375	0.03283
N_3 (1)	0.17877	0.05759	0.11207	0.05771
N_3 (2)	0.15653	0.05043	0.09813	0.05053
atrz (1)	0.00318	0.00102	0.00199	0.00103

[a] The Molecular fragments that provide electrons during excitation; [b] Molecular fragments that receive electrons during excitation; The unit for all data in the table is *e*.

Table S 5. Intrinsic charge transfer (CT) and local excitation (LE) percentage.

CT (74.157 %)				LE (25.843 %)	
MLCT (e)	LMCT (e)	LLCT (e)		MC (e)	LC (e)
0.12934	0.33848	0.27375		0.10169	0.15675

7. References

[1] Frisch, M. J.; Trucks, G. W.; Schlegel, H. B.; Scuseria, G. E.; Robb, M. A.; Cheeseman, J. R.; Scalmani, G.; Barone, V.; Petersson, G. A.; Nakatsuji, H.; Li, X.; Caricato, M.; Marenich, A. V.; Bloino, J.; Janesko, B. G.; Gomperts, R.; Mennucci, B.; Hratchian, H. P.; Ortiz, J. V.; Izmaylov, A. F.; Sonnenberg, J. L.; Williams-Young, D.; Ding, F.; Lipparini, F.; Egidi, F.; Goings, J.; Peng, B.; Petrone, A.; Henderson, T.; Ranasinghe, D.; Zakrzewski, V. G.; Gao, J.; Rega, N.; Zheng, G.; Liang, W.; Hada, M.; Ehara, M.; Toyota, K.; Fukuda, R.; Hasegawa, J.; Ishida, M.; Nakajima, T.; Honda, Y.; Kitao, O.; Nakai, H.; Vreven, T.; Throssell, K.; Montgomery, J. A. Jr.; Peralta, J. E.; Ogliaro, F.; Bearpark, M. J.; Heyd, J. J.; Brothers, E. N.; Kudin, K. N.; Staroverov, V. N.; Keith, T. A.; Kobayashi, R.; Normand, J.; Raghavachari, K.; Rendell, A. P.; Burant, J. C.; Iyengar, S. S.; Tomasi, J.; Cossi, M.; Millam, J. M.; Klene, M.; Adamo, C.; Cammi, R.; Ochterski, J. W.; Martin, R. L.; Morokuma, K.; Farkas, O.; Foresman, J. B.; and Fox. D. J. *Gaussian 16*, Revision A. 03, Gaussian. Inc., Wallingford CT **2016**, 3.

[2] Lu, T.; Chen, F. Multiwfn: A Multifunctional Wavefunction Analyzer. *J. Comput. Chem.* **2012**, 33, 580–592.

[3] Humphrey, W.; Dalke, A.; Schulten, K. VMD: Visual Molecular Dynamics. *J. Mol. Graph.* **1996**, 14, 33–38.